Materials Science & Engineering A 856 (2022) 144014

Contents lists available at ScienceDirect

Materials Science & Engineering A

journal homepage: www.elsevier.com/locate/msea

High temperature and strain-rate response of AA2124-SiC metal matrix composites

Xuan Li [a], Jin Kim [b], Anish Roy [b], Sabino Ayvar-Soberanis [c,*]

[a] Centre for Medical and Industrial Ultrasonics, James Watt School of Engineering, University of Glasgow, Glasgow, UK
[b] Wolfson School of Mechanical, Electrical and Manufacturing Engineering, Loughborough University, Loughborough, UK
[c] The University of Sheffield, Advanced Manufacturing Research Centre, Park Wallis Way, Catcliffe, Rotherham, UK

ARTICLE INFO

Keywords:
High strain rate
High temperature
AA2124-SiC MMC
SHPB
Microstructural analysis

ABSTRACT

This paper presents the results of the study of the dynamic impact behaviour of the AA2124-SiC Metal Matrix Composite (MMC) material with different particle reinforcement sizes and qualities using a compressive Split-Hopkinson Pressure Bar (SHPB) apparatus. Mechanical tests were performed at strain rates 1000 s^{-1}, 2000 s^{-1}, and 3000 s^{-1} and at temperatures of room temperature (25 °C), 100 °C and 200 °C. Microstructural analyses were carried out on the samples pre and post-compression experiments to study the fracture characteristics and mechanisms of the MMC materials. The flow stress-strain, strain rate, temperature effects and deformation mechanism were investigated. The backscattered electron images show that a higher strain rate of deformation induces the formation of denser and smaller grain size of $CuAl_2$ precipitates, especially in composites with smaller SiC particle sizes. Temperature has posed a minor effect on the microstructural change. Heating the samples close to a solution treatment temperature, and then followed by an air quenching has resulted in a fine dispersion of $CuAl_2$ precipitates, as well as a high saturation for the materials with a higher volumetric fraction of SiC reinforcement. The SHPB compression results reveal that the 225XF material has developed the highest stress among all materials. For materials with a higher volumetric fraction of SiC reinforcement (225XE and 225XF), cracks and failures have appeared in the samples during high strain rate and high-temperature compression experiments, which is believed to be caused by the increased brittleness of the material as a result of intensified oxide phases.

1. Introduction

Aluminium alloys exhibit excellent features such as lightweight, high thermal conductivity, and high corrosion resistance, presenting an increasing demand in the automotive and aerospace industries [1]. Dispersion of ceramic particles in a metallic matrix leads to significant improvements in stiffness and thermal resistance with a reduction in thermal conductivity. These classes of composite materials are referred to as particulate metal matrix composites (MMC).

An important factor that affects the mechanical properties of the MMC material is the morphology of the reinforcement. Three major classes of morphology are normally available: continuous fibre, chopped fibre or whisker, and particulate. Compared to the continuous or the whisker morphologies, the discontinuous reinforced aluminium is the most commonly used material in MMC material families, which provides a comparatively more moderate but isotropic increase in properties and typically affordable at the lowest cost for production. The reinforcement particle size is normally between 2 μm and 100 μm with a volumetric quantity of 1%–60% [2].

In terms of fabrication, stir casting, squeeze casting, compo-casting, infiltration, spray deposition, direct melt oxidation process and powder metallurgy are widely used for the aluminium metal matrix composites [3].

In this research, aerospace-grade aluminium alloy (AA2124) is investigated as the homogenous metal matrix, due to its formability, lightweight, good corrosion resistance [4] and relatively low cost compared to other lighter metals such as magnesium and titanium. From the matrix reinforcement perspective, materials used are typically ceramic as they provide a desirable combination of stiffness, strength, and relatively low density. The common candidate reinforcement materials include silicon carbide (SiC), aluminium oxide (Al_2O_3), boron carbide (B_4C), titanium carbide (TiC), titanium diboride (TiB_2), graphite

* Corresponding author.
E-mail address: s.ayvar@amrc.co.uk (S. Ayvar-Soberanis).

https://doi.org/10.1016/j.msea.2022.144014
Received 10 June 2022; Received in revised form 2 September 2022; Accepted 12 September 2022
Available online 17 September 2022

and a number of other ceramics [3,5–8].

Prior research indicates that the imposed deformation strain rates affect the mechanical properties and performance of the MMC materials. Many studies explore the mechanical properties of MMC at low strain rates using a conventional quasi-static method with a standard tensile machine [9,10]. However, the deformation of the material can is significantly altered when compressed at higher strain rates. For example, the inherent strain rate in ballistic impact experiments is of order 10^4 s^{-1}, and thus, is 6–7 orders of magnitude larger than typical values of 10^{-2} s^{-1} to 10^{-3} s^{-1} used in quasi-static tension tests [11]; in conventional metal cutting process, strain rate can easily reach to 10^5 s^{-1} [12], and during high impact machining processes, such as in ultrasonically assisted machining, the strain rate can exceed 10^6 s^{-1} to 10^7 s^{-1} [13–15]. Therefore, it highlights the importance to investigate the fracture and failure mechanism of the MMC materials at high strain rates and study the variation of the thermal effect.

Prior studies show that strain rates above 10^3 s^{-1} on the AA-SiC MMC materials have been successfully achieved [16], using a dynamic impact test apparatus called Split Hopkinson Pressure Bar, also known as a "Kolsky bar" [17]. It has been reported that the MMC material with the base aluminium 6061-T6 metal matrix presents an increased strength, but essentially the same strain hardening was observed. However, the rate sensitivity appears stronger than the unreinforced monolithic alloy at high strain rates [16,18]. Observation shows that as the increase in the volume fraction of the SiC particulate reinforcement, both yield strength and tensile strength increase but elongation decreases [19], which is due to a high volume fraction reinforced composites exhibiting high microstructural homogeneity and high hardness compared to low volume fraction reinforced composites [20]. The distribution and asperity of the hard SiC reinforcement in the soft metal matrix to external loading can also significantly affect the strength of the MMC materials [21]. Although the enhancements in yield strength can be attributed to the fine grain size of the metal matrix, there are also consistent reports demonstrating that the plastic response of the material is simultaneously degraded [4].

The above studies are primarily focused on the investigation of the effect on the mechanical properties of the MMC materials with a varying volumetric fraction of SiC reinforcement. However, the size of the SiC particles effect is not explored extensively, especially for sub-micron size SiC particulate embedded in the metal matrix. Additionally, the thermal effect on the mechanical properties of the MMC materials also remains unexplored in recent work, except in Ref. [22], which reports that flow stress varies nonlinearly with increasing temperature.

With the rapid development of MMC materials and the increasing demand from the industrial sectors, the mechanical properties of the MMC materials need to be further investigated at both quasi-static and high strain rate dynamic compression conditions. Hence, to bridge the gap in the literature for a comprehensive investigation of the fracture characteristics and mechanism of the AA-SiC Metal Matrix Composite materials, the research should include the study of the effects of different volumetric fractions of the reinforcement particulate elements, particle size, morphology, shape and temperature.

This research is focused on the study of the AA2124-SiC materials dynamic mechanical properties at different strain rates and temperatures, based on a number of samples with a different volumetric fraction of reinforcement particles, a range of different sizes and initial underlying microstructures. Flow stress-strain curves were recorded, and samples pre and post compression experiments were prepared for mechanical and microstructural analysis.

2. Experimental procedures

2.1. Materials

The materials used in this research, durable, lightweight SUPREMEX® metal matrix composites, are produced by Materion Aerospace Metal Composites, UK. To manufacture the MMCs, an ultrafine, homogeneously dispersed carbide reinforcement is combined with a high-quality aluminium alloy (AA2124) with a volumetric fraction of micron-sized SiC reinforcement, which is manufactured via a powder metallurgy route. Powder metallurgy is operated in the solid-state to minimize the chemical reaction between the metal matrix and the reinforcement SiC [23]. This method uses a high energy mixing process to pre-mix metal powder with ceramic reinforcement to form a composition prior to consolidation, ensuring a homogeneous distribution of the reinforcement and to refine the grain structure to enhance the mechanical properties.

Based on the reinforcement SiC particle size and the volumetric quantity, three types of AA2124-SiC MMC materials were available to use in this research, namely 217XG, 225XE and 225XF. The material properties of the MMC materials are provided by the supplier and are shown in Table I [24–26]

The supplied MMCs billets were cut with a bandsaw and then were wire electro discharge machined to produce a large quantity of cylindrical shape samples with a dimension Ø6 mm × 6 mm for high strain rate compression experiments.

2.2. Microstructural analysis

Microstructural analysis was conducted on the MMC samples pre and post compression tests at different strain rates and temperatures, using Field Emission Gun Scanning Electron Microscopy (FEGSEM) facility (JSM-F100, JEOL Ltd). To facilitate the analysis process, an additional wire erosion process was performed to slice the cylindrical samples along the central axis into two equal portions to provide an easy access to the surface of the cross-section. Thereafter, the cut samples were mounted on a thermally heated bakelite and followed by a polishing process to remove roughly 1 μm thickness using a polishing pad and fluid. During sample polishing, the applied force and rotational speed of the machine (Tegramin-30) were set to 22 N and 150 rpm, respectively. The secondary electron (SE) and backscattered electron (BSE) images were collected for all samples followed by an energy dispersive X-ray spectroscopy (EDS) analysis on the microstructure.

2.3. Dynamic impact test

The dynamic high strain rate impact experiments were performed for all MMC samples using a Split-Hopkinson Pressure Bar (SHPB) apparatus, which the detailed specifications in regard to the operation procedures can be found in Ref. [27]. The schematic representation of the SHPB apparatus is presented in Fig. 1.

The system consists of a gas launcher that accommodates a striker bar, an incident bar, a transmission bar, and a stopper mechanism, which are all aligned horizontally and mounted on a flat metal base. The bars are made from Maraging steel 350. The length of the incident bar and transmission bar is around 1828.8 mm (6″) with a diameter of 19.05 mm (0.75″). The gas launcher, which is charged with pressurised

Table 1
MMC material properties.

	217XG	225XE	225XF
Density ρ [kg/m^3]	860	2880	2880
Young's Modulus E [GPa]	98	115	115
Poisson's Ratio ν	0.3	0.3	0.3
Thermal Conductivity λ [W/m°K]	150	150	150
Thermal Expansion α [ppm/°C]	17.0	16.1	16
Solidus Temperature [°C]	548	548	548
Specific Heat Capacity c [J/g/°C]	0.848	0.848	0.848
Yield Strength $R_{p0.2}$ [MPa]	480	400	570
Tensile Strength R_m [MPa]	560	535	630
SiC size [μm]	0.3	3.0	0.7
SiC volume [%]	17	25 25	

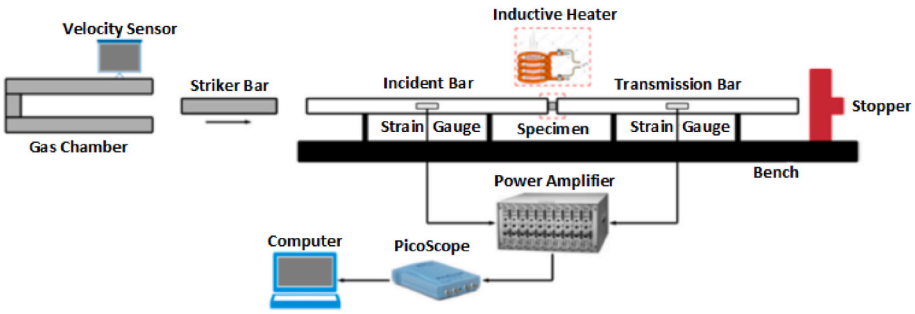

Fig. 1. Schematic representation of the SHPB system for high strain rate compression test.

gas accelerates a striker bar at an exit velocity measured with a speed sensor, creating an impact incident. The impact of the striker bar on the incident bar generates a stress pulse travelling within the incident bar at the speed of sound in Maraging steel 350, which is commonly known as "incident pulse". The pulse (a longitudinal wave) continues travelling within the incident bar to the sample, which is sandwiched concentrically between the incident bar and the transmission bar, generating a compression wave. Due to the impedance mismatch, part of the stress wave is reflected in the incident bar, known as "reflected pulse", and the rest of the stress wave is transmitted into the transmission bar, known as "transmitted pulse". The propagation of the stress wave then continues until the energy is fully dissipated.

Fig. 2 presents the SHPB experimental setup. To capture the pulse signals, two strain gauges with a resistance of 350 Ω (SGD-7/350-LY11, Omega Engineering) were attached to the centre of the length of the incident bar and transmission bar, respectively. The detected pulse signals were then supplied to a power amplifier (Vishay 2310B, Vishay Intertechnology), and the outputs were collected by an oscilloscope (PicoScope 4224, Pico Technology) and displayed in a computer. Stress, strain, and strain rate were then calculated from the captured signals using SurePulse software package (REL Inc). For high temperature dynamic compression tests, an induction heating unit (EASYHEAT, Ambrell Corporation) was used to heat up the samples before launching the striker bar. To ensure an accurate temperature during the impact, a K-type thermo-couple (KMQXL-IM300U-300), Omega Engineering) was inserted into the core of the sample to measure the temperature response against the heating up time and cooling time. The temperature signal was captured using a data logger (TC-08, Pico Technology).

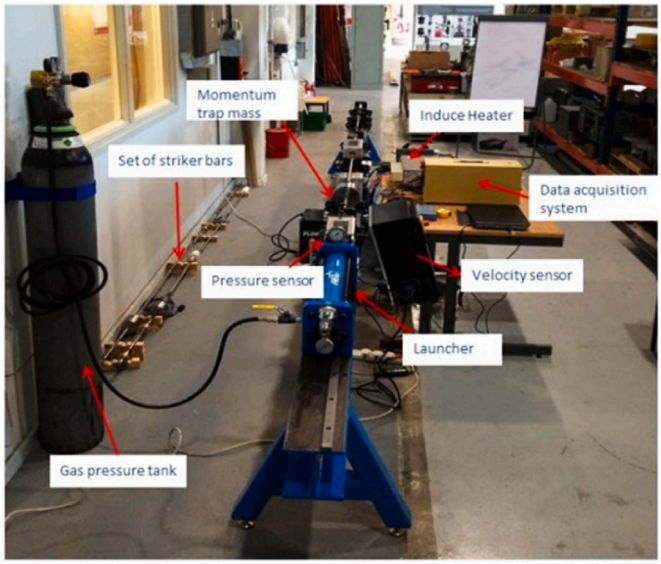

Fig. 2. SHPB experimental setup.

The target strain rates in experiments were set to 1000 s^{-1}, 2000 s^{-1} and 3000 s^{-1}, noting that a higher strain rate has caused the samples to shatter. The target temperatures on the samples were chosen to be room temperature (25 °C), 100 °C, and 200 °C, leaving the operator sufficient time to prepare for the impact incident (close the incident bar and the transmission bar to put the sample in position, and then launch the striker bar) once the sample was heated to a temperature close to the melting temperature of the samples (see Table I), allowing the temperature of the heated sample to cool (air quenching) to the target temperature the moment when the striker bar was fired.

3. Results and discussion

3.1. Microstructural analysis

Secondary electron images of the raw samples of the three types of the MMC materials (217XG, 225XE, and 225XF) are presented in Fig. 3.

Results show that 225XE material exhibits the largest particle size of SiC reinforcement, creating the largest SiC-free area filled with Al matrix with alloying elements. 217XG and 225XF materials present significantly smaller grain sizes of SiC reinforcement. 217XG has the lowest amount of SiC reinforcement, which is more sparsely embedded in the Al metal matrix. Due to solid-state manufacturing process with a controlled heat treatment, $CuAl_2$ precipitates are also dispersed sparsely in the metal matrix.

Backscattered electron (BSE) images (Fig. 4) using a full compositional mode were obtained for samples after the compression tests at two different strain rates (1000 s^{-1} and 3000 s^{-1}) and two different temperatures (25 °C and 200 °C). It should be noted that the BSE images could not be collected for samples at a 3000 s^{-1} strain rate and a 200 °C temperature because of the crack/shatter samples (see Fig. 5), which happened for all three materials.

In general, a higher strain rate has resulted in denser and smaller size of $CuAl_2$ precipitates due to a larger deformation in the samples, especially for the materials with small particle sizes (217XG and 225XF). This observation has been confirmed in Fig. 6 from the EDS analysis of the $CuAl_2$ component. Moreover, the microstructures indicate that heat generation during high strain rate deformation has posed a minor effect on the microstructural change. The microstructures at 200 °C show a fine dispersion of $CuAl_2$ precipitation, causing a high saturation of the precipitation for 225XE and 225XF material. This can be observed more clearly from the EDS analysis of $CuAl_2$ component in Fig. 7. However, 217XG shows a reduced amount of finely dispersed precipitation, suggesting a lower amount of SiC particles has hindered alloying constituents to be transformed into solution.

Additionally, from the EDS analysis of the compressed samples in Fig. 8, it can also be observed that oxide phases have intensified in the thermally treated samples, forming brittle oxide phases. At the highest strain rate (3000 s^{-1}) with room temperature (25 °C), the oxide phases have been enhanced, especially for the MMC samples with a higher volumetric fraction of SiC reinforcement. For the 225XE material, with the highest volumetric fraction of SiC and the largest SiC particle size,

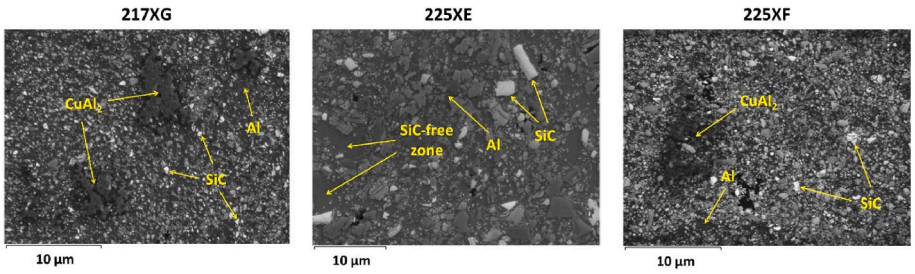

Fig. 3. Secondary electron (SE) images of raw samples (pre-compression) of 217XG, 225XE and 225XF materials.

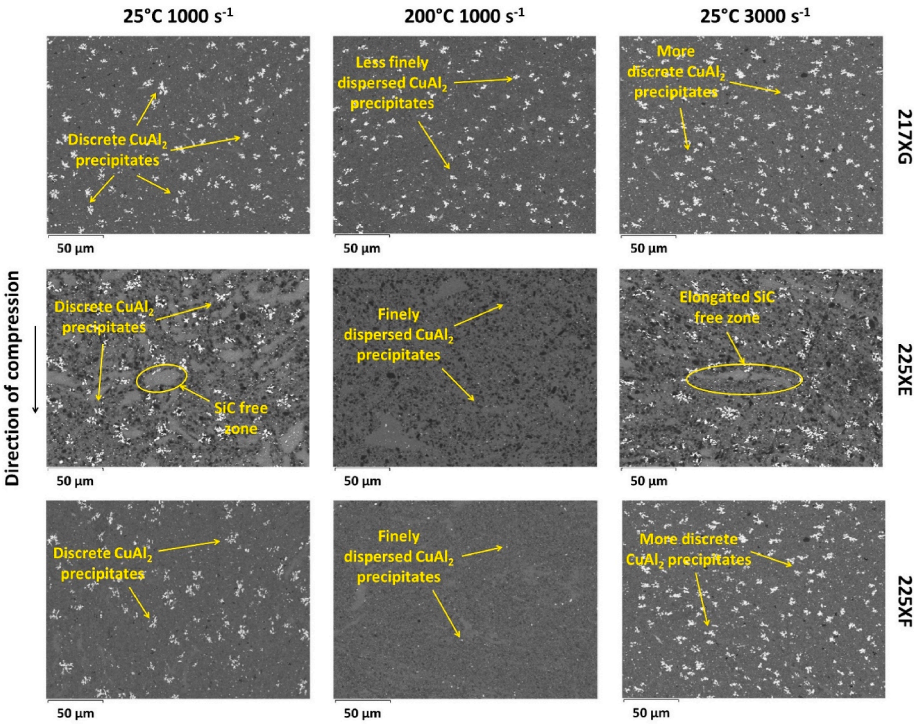

Fig. 4. Backscattered electron (BSE) images of the compressed samples (post-compression) of 217XG, 225XE and 225XF materials at 1000 s^{-1} and 3000 s^{-1} strain rates, and at 25 °C and 200 °C temperatures.

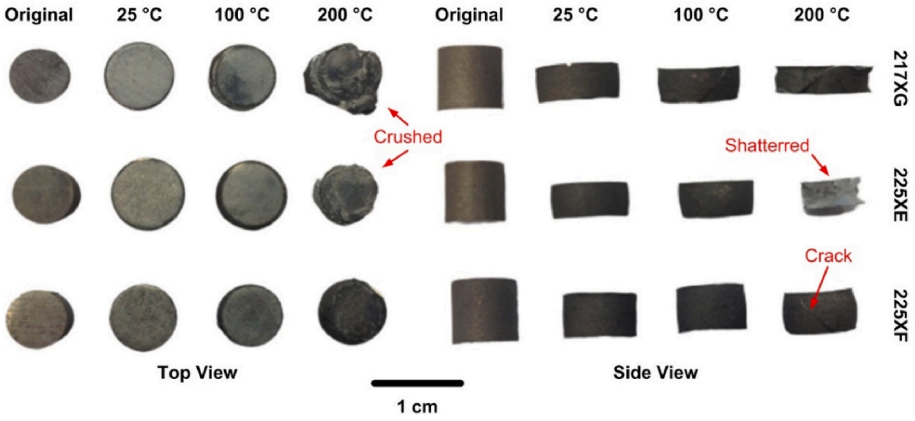

Fig. 5. MMC Samples pre and post a high strain rate (3000 s^{-1}) compression impact of original shape as an example, at 25 °C, 100 °C, and 200 °C temperature.

there is a line of oxidation observed, which could potentially be the origin of the weak bonding area in the Al matrix and can cause samples to start to develop cracks. Indeed, a high strain rate (3000 s^{-1}) and a temperature of 200 °C have resulted in fractures/cracks in the MMC samples due to crack propagation initiated from brittle oxide phases or SiC particle fracture (see Fig. 5).

Table II illustrates the change in weight in percentage for the elements of all material samples at selected strain rates and temperatures.

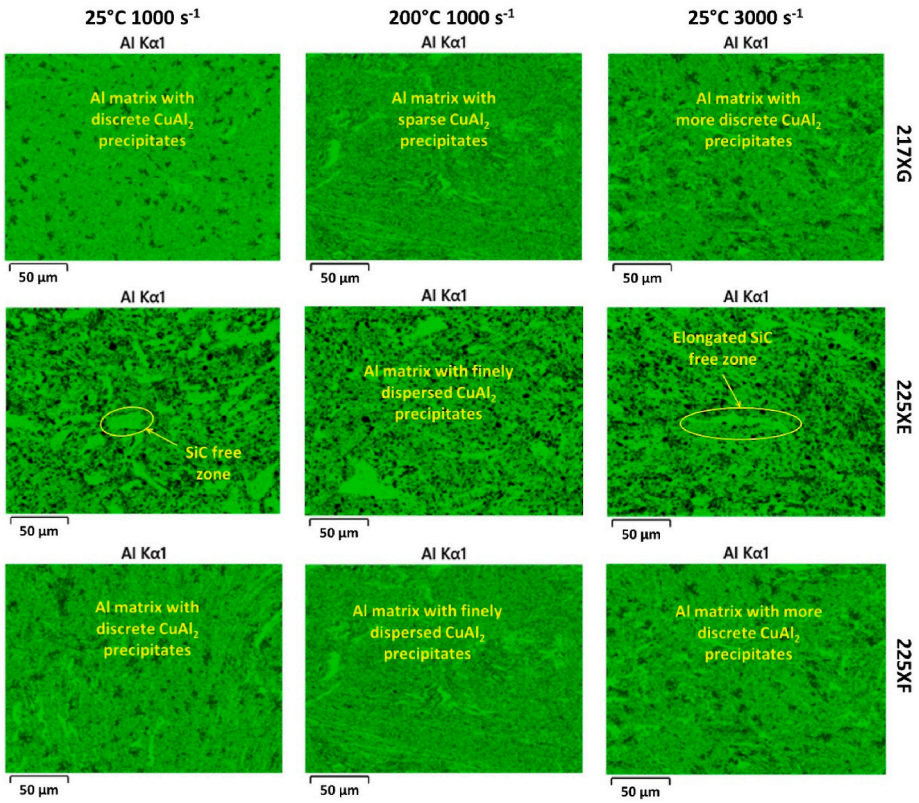

Fig. 6. Energy dispersive X-ray spectroscopy (EDS) images of the compressed samples (post-compression) of 217XG, 225XE and 225XF materials for the component of Al at 1000 s^{-1} and 3000 s^{-1} strain rates, and 25 °C and 200 °C temperature.

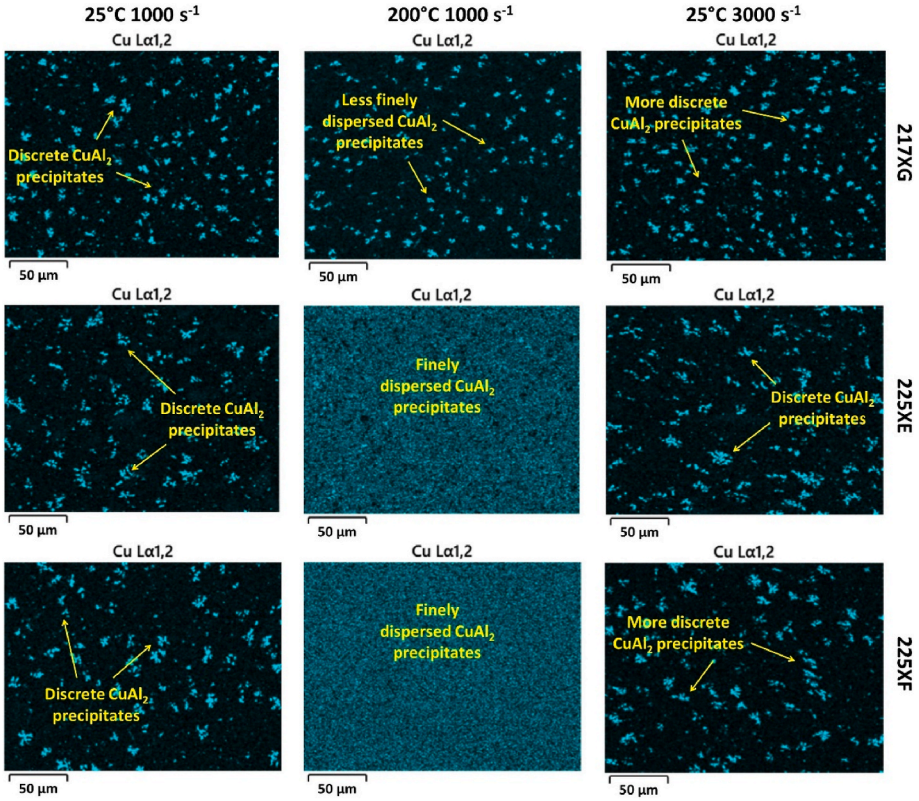

Fig. 7. Energy dispersive X-ray spectroscopy (EDS) images of the compressed samples (post-compression) of 217XG, 225XE and 225XF materials for the component of $CuAl_2$ at 1000 s^{-1} and 3000 s^{-1} strain rates, and 25 °C and 200 °C temperature.

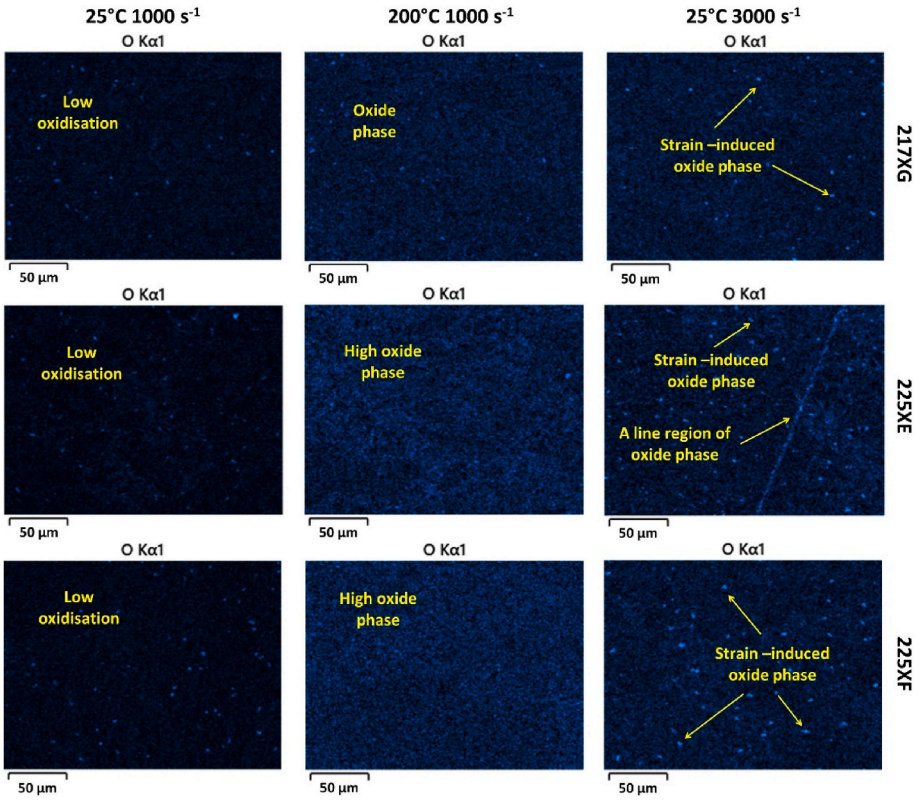

Fig. 8. Energy dispersive X-ray spectroscopy (EDS) images of the compressed samples (post-compression) of 217XG, 225XE and 225XF materials for the oxidation at 1000 s^{-1} and 3000 s^{-1} strain rates, and 25 °C and 200 °C temperature.

Table 2
Weight in percentage [%] of elements of MMC materials from energy dispersive X-Ray spectroscopy (EDS) analysis.

217XG	Carbon (C)	Oxygen (O)	Magnesium (Mg)	Aluminium (Al)	Silicon (Si)	Manganese (Mn)	Copper (Cu)
25 °C 1000s^{-1}	9.39	1.64	0.98	71.00	13.87	0.38	2.74
25°C 3000s^{-1}	9.47	1.69	1.00	70.24	14.01	0.44	3.15
200°C 1000s^{-1}	9.26	1.63	1.05	70.60	13.74	0.40	3.33
225XE	Carbon (C)	Oxygen (O)	Magnesium (Mg)	Aluminium (Al)	Silicon (Si)	Manganese (Mn)	Copper (Cu)
25 °C 1000s^{-1}	11.29	1.43	1.12	61.13	21.13	0.37	3.53
25°C 3000s^{-1}	11.77	1.30	0.67	61.64	21.42	0.37	2.83
200°C 1000s^{-1}	11.03	1.31	0.82	63.81	19.92	0.33	2.78
225XF	Carbon (C)	Oxygen (O)	Magnesium (Mg)	Aluminium (Al)	Silicon (Si)	Manganese (Mn)	Copper (Cu)
25 °C 1000s^{-1}	11.72	1.45	0.70	63.18	20.41	0.24	2.29
25 °C 3000s^{-1}	11.79	1.57	0.79	62.52	20.38	0.32	2.63
200°C 1000s^{-1}	11.66	1.31	0.82	62.75	20.09	0.27	3.09

Observed from the EDS spectrum, 217XG presents the lowest amount of Si and C and the highest composition of Al elements, compared to 225XE and 225XF, confirming the material properties in **Table I**. Both 217XG and 225XF, with finer particle sizes (0.3 µm and 0.7 µm), have resulted in an increase in Cu at a higher strain rate and higher temperature. 225XE material, with a coarser particle size (3.0 µm), has shown a decrease in Cu. These observations are consistent with the observation in Fig. 7.

Ideally, the weight of all elements should remain unchanged throughout the experiments, despite the change in strain rate and temperature.

3.2. Flow stress-strain characteristics

3.2.1. Striker bar velocity

Five different lengths striker bars were available in experiments, namely 50.8 mm (2″), 76.2 mm (3″), 152.4 mm (6″), 228.6 mm (9″), and 304.8 mm (12″). The diameter of these striker bars is 19.05 mm (0.75”), which is the same diameter as the incident bar and transmission bar, to avoid uneven distribution of the impact stress in the bars.

Fig. 9 presents the velocity of different lengths of striker bars exiting the gas chamber at different gas pressure levels, measured by a velocity sensor.

Unsurprisingly, the velocity of the striker bar increases as the increase in gas pressure. However, a longer striker bar has resulted in a reduction in velocity at the same gas pressure, due to the larger mass.

In practice, a shorter striker bar imparts a shorter time duration of impact with the incident bar, creating a pulse with sharper characteristic and producing a higher strain rate. As a comparison, the output signal of the strain gauge would exhibit a longer duration of pulse with a much flatter response if a longer striker bar were used. Choosing a proper length of striker bar for the impact experiment will depend on the target strain rate in the sample. The strain rate is calculated as an average of the integration of the pulsed curve of the stress wave signal as a function of impact time.

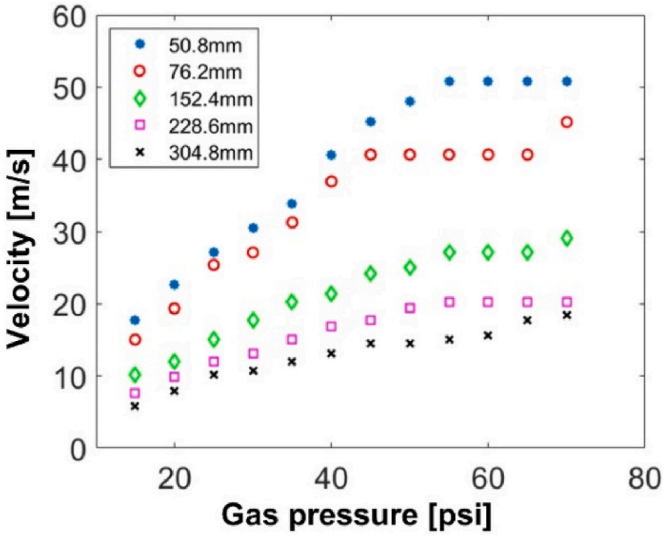

Fig. 9. Striker bar velocity with different gas pressure.

3.2.2. Dynamic compression test

In this section, the results of the dynamic compression test on the 217XG, 225XE and 225XF samples at different strain rates and temperatures are presented and discussed.

Fig. 10 shows the dynamic compression stress-strain characteristics for all MMC samples, tested at 1000 s^{-1}, 2000 s^{-1} and 3000 s^{-1} strain rates, and 25 °C, 100 °C and 200 °C temperatures.

In general, 225XF material sustains the highest stress, followed by 217XG and 225XE, regardless of the strain rates and temperatures. It has been observed that generally, the flow stress grows with the increase in the strain rate posed on all samples, demonstrating a strain rate hardening effect. This work has demonstrated that the manufactured AA2124-SiC MMC materials offer high strength and stiffness, refer to Fig. 10. The dynamic behaviour of a specific type of MMC material is insensitive to the change of temperature, except for the 200 °C temperature at 2000 s^{-1} and 3000 s^{-1} strain rates for the 225XF material, which show a noticeable thermal softening phenomenon. However, this thermal softening response is partially attributed to the internal crack initialisation of the sample due to the enhanced oxide phases at high temperatures and high strain rates, as shown in Figs. 5 and 8, respectively.

Elastic modulus values are estimated from the linear region of the stress-strain curves in Fig. 10 and are presented in **Table III**.

In general, the values appear stochastic for the change in strain rates and temperature for all MMC materials. At low strain rate (1000 s^{-1}), the elastic modulus exhibits small changes at different temperatures except for 225XE at 25 °C, which demonstrated a drastic decline when the sample was heated up. However, as the strain rate is increased to 2000 s^{-1}, the elastic modulus value rises as the sample heats up, especially from 25 °C to 100 °C, suggesting the material hardens at a higher strain rate and a higher temperature. This could be due to the intensified oxide phases in the MMC samples as presented in Fig. 8, which has resulted in an increased brittleness of the material and promoted the mechanical strength. Finally, all materials show softening

Table 3
Elastic modulus (GPa) of MMC samples at different strain rates and temperatures with standard deviation.

1000 s^{-1}	217XG	225XE	225XF
25°C	34.2 ± 1.5	163.7 ± 9.7	63.7 ± 21
100°C	98.2 ± 20.6	94.4 ± 6.5	72.9 ± 0.3
200°C	75.2 ± 7	54 ± 4.7	67.3 ± 0.9
2000 s^{-1}	**217XG**	**225XE**	**225XF**
25°C	26 ± 3.9	38.7 ± 4.5	30.3 ± 4.4
100°C	122.5 ± 35.2	271.5 ± 17.8	98.3 ± 42.8
200°C	78.1 ± 13.3	58.4 ± 25.1	77.9 ± 11.8
3000 s^{-1}	**217XG**	**225XE**	**225XF**
25°C	25.5 ± 0.1	21.6 ± 2.3	40.7 ± 19.9
100°C	49.8 ± 16.8	122.9 ± 8.8	39.7 ± 10.5
200°C	40.8 ± 5.3	42.3 ± 1.2	76.9 ± 2.2

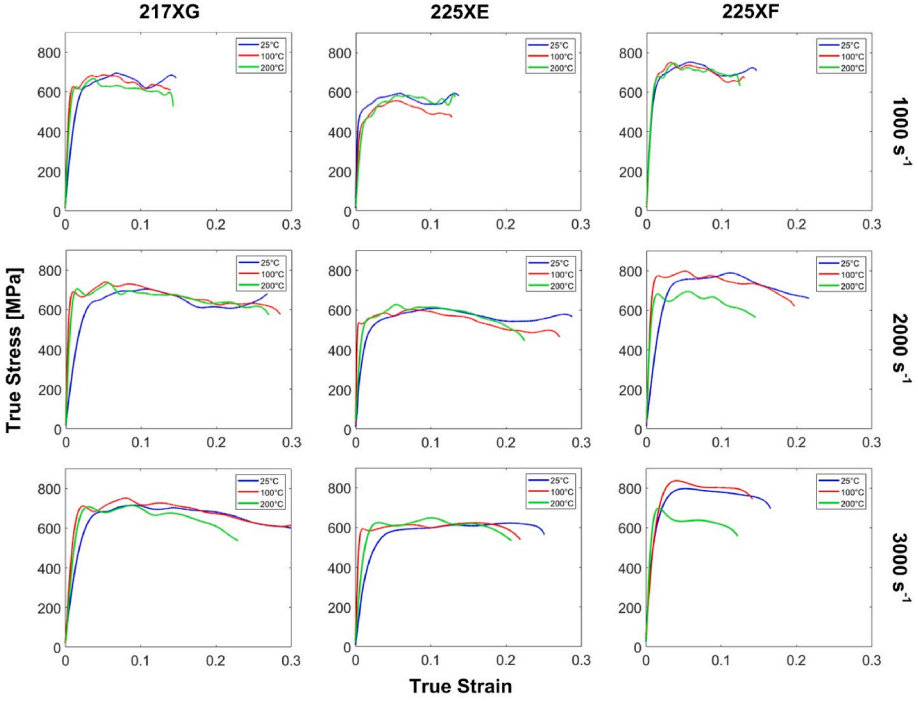

Fig. 10. True stress-strain characteristics of the 217XG, 225XE and 225XF samples tested at 1000 s^{-1}, 2000 s^{-1}, 3000 s^{-1} and at temperatures of 25 °C, 100 °C and 200 °C.

characteristics as the strain rate is increased to 3000 s^{-1}.

In terms of deformation, at 1000 s^{-1} strain rate, the unloading takes place at around 15% of the true strain, and this value increases to 30% for the 2000 s^{-1} and 3000 s^{-1} strain rates. However, exceptions are present for 225XF at 2000 s^{-1} and 3000 s^{-1}, and 225XE at 3000 s^{-1} strain rates, with 10%–20% deformation are reported. This again, is related to the intensified brittle oxide phases in the MMC material, causing small cracks to initiate, therefore reduced the maximal compression of the sample.

From Table IV, a significant increase in the mechanical strength is observed as the particle size of the SiC reinforcement becomes smaller (217XG 0.3 μm SiC size, 225XE 3.0 μm SiC size, and 225XF 0.7 μm SiC size), suggesting finer SiC components can form a stronger.

Bonding within the Al matrix. The yield strength of the material is considerably enhanced as the increase in the volumetric fraction of the SiC reinforcement, for sub-micron particle size of SiC. A higher temperature has produced a slightly higher yield strength in the MMC material; however, the difference is small for 100 °C and 200 °C. Variation in the mechanical strength is the highest for 225XF at 2000 s^{-1} and 3000 s^{-1} strain rates, which again, is related to the crack propagation, making the dynamic response of the material more inconsistent and unrepeatable.

It should be emphasised that samples were heated up to their solidus temperature of 500 °C and then were cooled down, which has resulted in a change in microstructure, causing the samples to become harder when the impact event took place. Also, 200 °C might not be a high enough temperature to detect any thermal softening effect due to the high thermal diffusivity and formation of fine $CuAl_2$ precipitation and oxidised grains.

According to the values in Table IV, it is clear that a lower strain rate (1000 s^{-1}) has only caused small changes in yield strength, indicating that the particles only start to interact intensely at higher strain rates (2000 s^{-1} and 3000 s^{-1}). This means that thermal softening of the matrix has become meaningless at high compressive strain (unless the particles are also thermally softened).

It was also discovered from experiments that a shorter bar had to be used to achieve the prescribed level of strain rate for a higher target mechanical strength, which has reduced the total deformation of the sample (2000 s^{-1} and 3000 s^{-1} strain rates in Fig. 10). Additionally, 225XE and 225XF material samples were fractured (see Fig. 5), as a result of a higher volumetric fraction of the SiC reinforcement, presenting a higher brittleness in the material because of the enhanced oxide phases (Fig. 8). This explains the observation of the unloading emerging at a much smaller deformation (<20%) for the 225XF sample at a 3000 s^{-1} strain rate.

4. Conclusion

A study of the dynamic impact behaviour and microstructure analysis of AA2124-SiC Metal Matrix Composite material with different SiC particle sizes and volumetric fraction is presented, aimed to understand the thermal softening and strain rate sensitivity effects and fracture mechanisms of the MMC materials.

Microstructure analysis of the raw samples suggests that 225XE shows the largest particle size of SiC reinforcement (nominal size 3.0 μm and 25% in volume), leaving the greatest SiC-free zone which is filled with AA2124 alloying elements. $CuAl_2$ precipitates are dispersed sparsely within the metal matrix, because of solid-state manufacturing and controlled heat treatment.

Backscattered electron images indicate that a higher strain rate (3000 s^{-1}) has produced denser and smaller size of $CuAl_2$ precipitates due to a higher deformation of the MMC samples, especially for the materials with small particle sizes (217XG and 225XF). The images also show that the microstructures at a temperature of 200 °C have a fine dispersion of $CuAl_2$ precipitates, causing a high saturation of precipitation in materials with a larger volumetric fraction of SiC (225XE).

Table 4
Yield strength (MPa) of MMC samples at different strain rates and temperatures with standard deviation.

1000 s^{-1}	217XG	225XE	225XF
25°C	543 ± 7.5	469 ± 3	604 ± 26
100°C	606 ± 17.5	417 ± 6	645 ± 14.5
200°C	593 ± 8.5	438 ± 2	652 ± 2.5
2000 s^{-1}	**217XG**	**225XE**	**225XF**
25°C	542 ± 3	441 ± 16	662 ± 12.5
100°C	668 ± 30.5	536 ± 11	727 ± 42
200°C	669 ± 29	524 ± 12	660 ± 30
3000 s^{-1}	**217XG**	**225XE**	**225XF**
25°C	569 ± 1	429 ± 5	620 ± 40
100°C	642 ± 58	583 ± 1	727 ± 29.5
200°C	635 ± 15	515 ± 9	646 ± 52

Moreover, it was observed that oxide phases were intensified with thermally treated samples, forming brittle oxide phases. The highest strain rate (3000 s^{-1}) with the highest temperature 200 °C combination has generated fractures in 225XE and 225XF samples due to crack propagation initiated from brittle oxide phases or SiC particle fracture.

Among all materials tested in the compression experiments, the elastic modulus of the materials shows thermal hardening characteristics, however, they appear insensitive to the increase in strain rate. 225XF has demonstrated the highest yield strength, and temperature has posed a minor effect on the stress levels of the MMC samples.

To improve the mechanical strength and reduce the brittleness of the MMC samples, a small particle size and a large volume of SiC reinforcement in the Al matrix are desired (225XF, for instance). Furthermore, the obtained flow stress of the MMC materials appears insensitive to the change in temperature, increasing the feasibility of the materials to be used in a high-temperature environment, such as in automotive and aero engines, where traditional metal alloy materials suffer. However, the brittleness is significantly increased at a high strain rate (3000 s^{-1}) and 200 °C, especially for high volumetric fraction and large size SiC particle MMC materials (225XE and 225XF), making the application more challenging.

CRediT authorship contribution statement

Xuan Li: Methodology, Software, Validation, Formal analysis, Investigation, Resources, Data curation, Writing – original draft, Writing – review & editing, Visualization, Supervision, Project administration. **Jin Kim:** Methodology, Software, Validation, Formal analysis, Investigation, Resources, Data curation, Writing – original draft, Visualization, Project administration. **Anish Roy:** Conceptualization, Methodology, Resources, Writing – review & editing, Supervision, Project administration, Funding acquisition. **Sabino Ayvar-Soberanis:** Conceptualization, Methodology, Resources, Writing – review & editing, Supervision, Project administration, Funding acquisition.

Declaration of competing interest

The authors declare that they have no known competing financial interests or personal relationships that could have appeared to influence the work reported in this paper.

Data availability

Data will be made available on request.

Acknowledgement

This work was supported by the EPSRC Programme Grant (H2 Manufacturing: Hybrid-Hybrid machining of next generation aerospace materials) under Grant EP/P027652/1 and EP/P027555/1. The authors

also thank the Advanced Manufacturing Research Centre (AMRC) for allowing the use of the Split-Hopkinson Pressure Bar apparatus and are grateful for the access to the Loughborough Materials Characterisation Centre for performing all microstructure analysis.

References

[1] S.T. Mavhungu, E.T. Akinlabi, M.A. Onitiri, F.M. Varachia, Aluminum matrix composites for industrial use: advances and trends, Procedia Manuf. 7 (2017) 178–182.
[2] M. Zadra, L. Girardini, High-performance, low-cost titanium metal matrix composites, Mater. Sci. Eng., A 608 (2014) 155–163.
[3] T.P.D. Rajan, R.M. Pillai, B.C. Pai, Reinforcement coatings and interfaces in aluminium metal matrix composites, J. Mater. Sci. 33 (14) (1998) 3491–3503.
[4] N. Behm, H. Yang, J. Shen, K. Ma, L.J. Kecskes, E.J. Lavernia, J.M. Schoenung, Q. Wei, Quasi-static and high-rate mechanical behavior of aluminum-based MMC reinforced with boron carbide of various length scales, Mater. Sci. Eng., A 650 (2016) 305–316.
[5] T. Iseki, T. Kameda, T. Maruyama, Interfacial reactions between SiC and aluminium during joining, J. Mater. Sci. 19 (1984) 1692–1698.
[6] T. Nukami, M.C. Flemings, In situ synthesis of TiC particulate-reinforced aluminum matrix composites, Metall. Mater. Trans. 26 (7) (1995) 1877–1884.
[7] M.K. Aghajanian, M.A. Rocazella, J.T. Burke, S.D. Keck, The fabrication of metal matrix composites by a pressureless infiltration technique, J. Mater. Sci. 26 (2) (1991) 447–454.
[8] F. Ogawa, C. Masuda, Microstructure evolution during fabrication and microstructure-property relationships in vapour-grown carbon nanofibre-reinforced aluminium matrix composites fabricated via powder metallurgy, Composites Part A 71 (2015) 84–94.
[9] M. Guden, I.W. Hall, Quasi-static and dynamic compression behaviour of an FP^{TM} alumina-reinforced aluminium metal matrix composite, J. Mater. Sci. 33 (13) (1998) 3285–3291.
[10] M. Dong, S. Schmauder, T. Bidlingmaier, A. Wanner, Prediction of the mechanical behaviour of short fiber reinforced MMCs by combined cell models, Comput. Mater. Sci. 9 (1997) 121–133.
[11] S.L. Phoenix, U. Heisserer, H. van der Werff, M. van der Jagt-Deutekom, Modeling and experiments on ballistic impact into UHMWPE yarns using flat and saddle-nosed projectiles, Fibers 5 (8) (2017) 1–41.
[12] K. Zhang, K. Wang, Z. Liu, X. Xu, Strain rate of metal deformation in the machining process from a fluid flow perspective, Appl. Sci. 10 (9) (2020) 1–11.
[13] B. Wang, Z. Liu, G. Su, Q. Song, X. Ai, Investigations of critical cutting speed and ductile-to-brittle transition mechanism for workpiece material in ultra-high speed machining, Int. J. Mech. Sci. 104 (2015) 44–59.
[14] H. Hocheng, N.H. Tai, C.S. Liu, Assessment of ultrasonic drilling of C/SiC composite material, Composites Part A 31 (2) (2000) 133–142.
[15] T. Tawakoli, B. Azarhoushang, Influence of ultrasonic vibrations on dry grinding of soft steel, Int. J. Mach. Tool Manufact. 48 (14) (2008) 1585–1591.
[16] S. Yadav, D.R. Chichili, K.T. Ramesh, The mechanical response of a 6061-T6 Al/$A1_2O_3$ metal matrix composite at high rates of deformation, Acta Metall. Mater. 43 (12) (1995) 4453–4464.
[17] B. Hopkinson, A method of measuring the pressure produced in the detonation of high, explosives or by the impact of bullets, Phil. Trans. Math. Phys. Eng. Sci. 213 (497–508) (1914) 437–456.
[18] I. Tirtom, M. Güden, H. Yildiz, Simulation of the strain rate sensitive flow behavior of SiC-particulate reinforced aluminum metal matrix composites, Comput. Mater. Sci. 42 (4) (2008) 570–578.
[19] M. Song, Effects of volume fraction of SiC particles on mechanical properties of SiC/Al composites, Trans. Nonferrous Metals Soc. China 19 (6) (2009) 1400–1404.
[20] A.A. Iqbal, N. Amierah, Effect of reinforcement volume fraction on the mechanical properties of the Al-SiC nanocomposite materials, IOP Conf. Ser. Mater. Sci. Eng. 226 (2017) 1–9.
[21] R.A.G. Lezcano, E.J.L. Fernandez, S.C. Garcia, G.S. Contreras, Influence of strain rate on metal matrix composites, Contemporary Engineering Sciences 13 (1) (2020) 103–111.
[22] Y. Suo, J. Li, Z. Deng, B. Wang, Q. Wang, D. Ni, P. Jia, T. Suo, High-temperature compressive response of SiC_p/6092Al composites under a wide range of strain rates, Materials 14 (21) (2021) 1–15.
[23] D. Hashiguchi, D. Tricker, A. Tarrant, J. Campbell, C. Pokross, Discontinuously reinforced aluminum MMC extrusions, Met. Powder Rep. 72 (4) (2017) 252–258.
[24] 217XG Materion Datasheet - SupremEX®. https://www.rsalloys.eu/cms-admin/materiale/add_allegati/file-294-109-L1/supremex-217xg-data-sheet-8-15.pdf.
[25] 225XE Materion Datasheet - SupremEX®. https://materion.com/-/media/files/aerospace-metal-composites/supremex/supremex-225xe-data-sheet-915j.pdf.
[26] 225XF Materion Datasheet - SupremEX®. https://materion.com/-/media/files/aerospace-metal-composites/supremex/supremex-retainer-product-brief-2021-05-21.pdf.
[27] SHPB Calibration Manual and Sample Test (Compression)," REL SURE-Pulse, Calumet, MI, USA.